

Fig. 2. Cornering characteristics of front and rear tires. Dotted line: high-friction road, and dashed line: low-friction road.

left rear tires, while F_{yfr} and F_{yrr} are the cornering forces for the right front and right rear tires. F_{xfl} and F_{xrl} are the traction forces for the left front and left rear tires, while F_{xfr} and F_{xrr} are the traction forces for the right front and right rear tires.

We assume the vehicle body is symmetric about the longitudinal plane. Let $F_{yf} = F_{yfl} + F_{yfr}$, $F_{yr} = F_{yrl} + F_{yrr}$, $F_{xf} = F_{xfl} + F_{xfr}$, and $F_{xr} = F_{xrl} + F_{xrr}$. The basic equations of motion for steering dynamics with roll motion neglected were derived (e.g., [19]) and given as

$$m(\dot{\nu} - \nu\beta\gamma) = F_{xf} + F_{xr} - F_{yf} \sin \delta_f \quad (1)$$

$$m\nu \cdot (\dot{\beta} + \gamma) = F_{yf} + F_{yr} + F_{xf} \sin \delta_f \quad (2)$$

and

$$I_z \dot{\gamma} = (L_f F_{yf} - L_r F_{yr}) \cos \beta + L_f F_{xf} \sin \delta_f \quad (3)$$

where m is the mass of the vehicle, I_z is the yaw moment around z -axis, and ν is the longitudinal velocity.

In this paper, we focus on the characteristic analysis of lateral dynamics by assuming $F_{xf} = 0$, and the vehicle is not accelerating or decelerating along the longitudinal direction, i.e., $\dot{\nu} = 0$. Thus, (1) can then be neglected in this analysis. The steering dynamics for constant speed ν can then be reduced to a second-order model as given by

$$\dot{\beta} = \frac{1}{m\nu} \{F_{yf} + F_{yr}\} - \gamma \quad (4)$$

$$\dot{\gamma} = \frac{1}{I_z} \{L_f F_{yf} - L_r F_{yr}\} \cos \beta \quad (5)$$

where F_{yf} is a function of β , γ , and δ_f , and F_{yr} is a function of β and γ only. Examples of F_{yf} and F_{yr} are given in (21) and (22).

III. STABILITY AND BIFURCATION ANALYSIS

Here, we will study the vehicle steering dynamics by using the second-order model given by (4) and (5) instead of (1)–(3). Details are given as follows.

TABLE I
VEHICLE PARAMETERS AND VALUES

Symbol and description	Values
m : vehicle mass	1500 kg
I_z : yaw moment	3000 kg.m ²
ν : velocity	10 ~ 40 m/s
L_f	1.2 m
L_r	1.3 m

TABLE II
COEFFICIENTS OF MAGIC FORMULA

Symbol	High friction road	Low friction road
B_f, B_r	6.7651, 9.0051	11.275, 18.631
C_f, C_r	1.3, 1.3	1.56, 1.56
D_f, D_r	-6436.8, -5430	-2574.7, -1749.7
E_f, E_r	-1.999, -1.7908	-1.999, -1.7908

A. Stability Analysis

Define $x^0 = (\beta^0, \gamma^0)^T$ as an equilibrium point of system (4), (5) for a given $\delta_f = \delta_f^0$. We then have

$$F_{yf}(\beta^0, \gamma^0, \delta_f^0) + F_{yr}(\beta^0, \gamma^0, \delta_f^0) = \gamma^0 \cdot m\nu \quad (6)$$

and

$$L_f F_{yf}(\beta^0, \gamma^0, \delta_f^0) = L_r F_{yr}(\beta^0, \gamma^0, \delta_f^0) \quad (7)$$

or

$$\cos \beta^0 = 0. \quad (8)$$

Consider the condition as given in (8), we have $\beta^0 = n\pi + \pi/2$ for $n = 0, 1, 2, \dots$. It is clear that this condition cannot be achieved for a vehicle. Thus, the equilibrium point x^0 should satisfy the two conditions given in (6) and (7) only.

Let $x = [\beta, \gamma]^T$ and $\tilde{x} = x - x^0$. Taking the linearization of system (4), (5) at $x = x^0$, we have

$$\dot{\tilde{x}} = A\tilde{x} \quad (9)$$

where

$$A = \begin{bmatrix} a_1 & a_2 \\ a_3 & a_4 \end{bmatrix} \quad (10)$$

with

$$a_1 = \frac{1}{m\nu} \frac{\partial}{\partial \beta} (F_{yf} + F_{yr})(\beta^0, \gamma^0, \delta_f^0) \quad (11)$$

$$a_2 = \frac{1}{m\nu} \frac{\partial}{\partial \gamma} (F_{yf} + F_{yr})(\beta^0, \gamma^0, \delta_f^0) - 1 \quad (12)$$

$$a_3 = \frac{1}{I_z} \left(L_f \frac{\partial F_{yf}(\beta^0, \gamma^0, \delta_f^0)}{\partial \beta} - L_r \frac{\partial F_{yr}(\beta^0, \gamma^0, \delta_f^0)}{\partial \beta} \right) \cos \beta^0 \quad (13)$$

and

$$a_4 = \frac{1}{I_z} \left(L_f \frac{\partial F_{yf}(\beta^0, \gamma^0, \delta_f^0)}{\partial \gamma} - L_r \frac{\partial F_{yr}(\beta^0, \gamma^0, \delta_f^0)}{\partial \gamma} \right) \cos \beta^0. \quad (14)$$

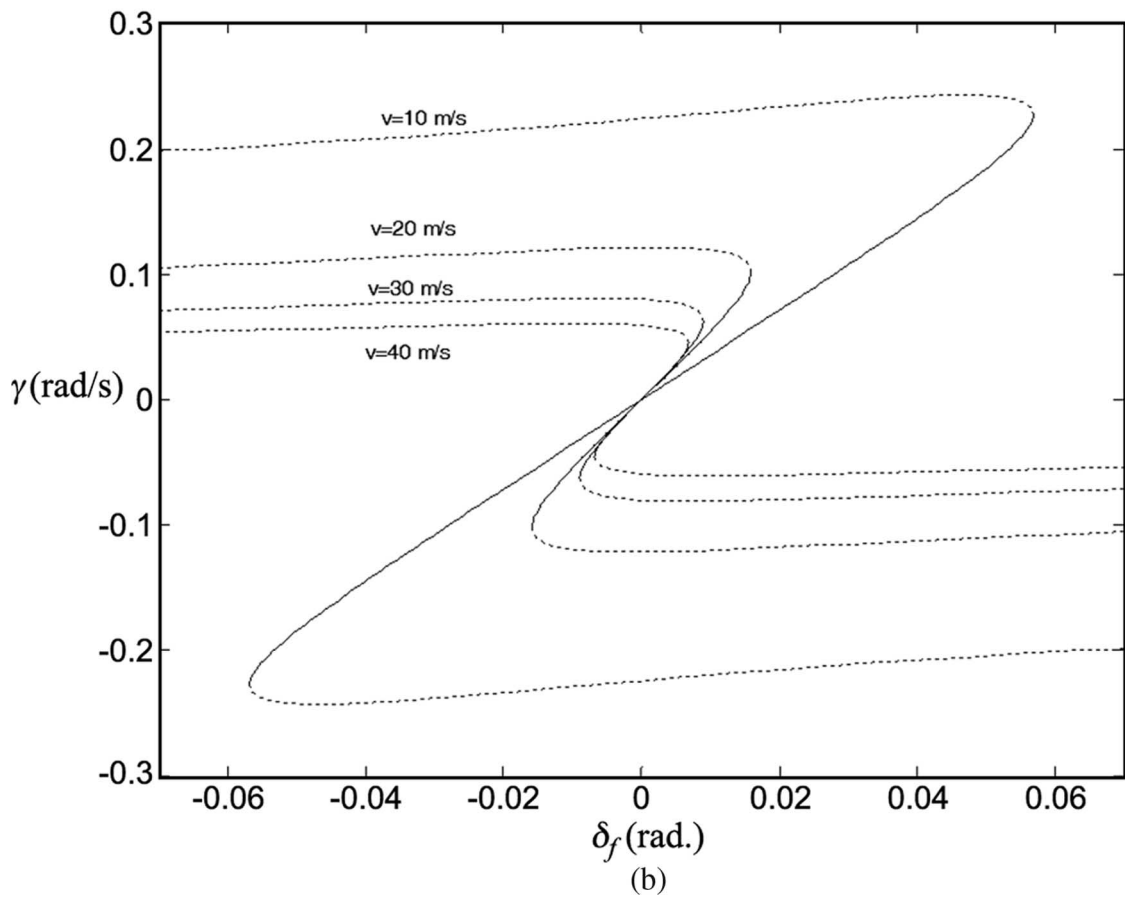
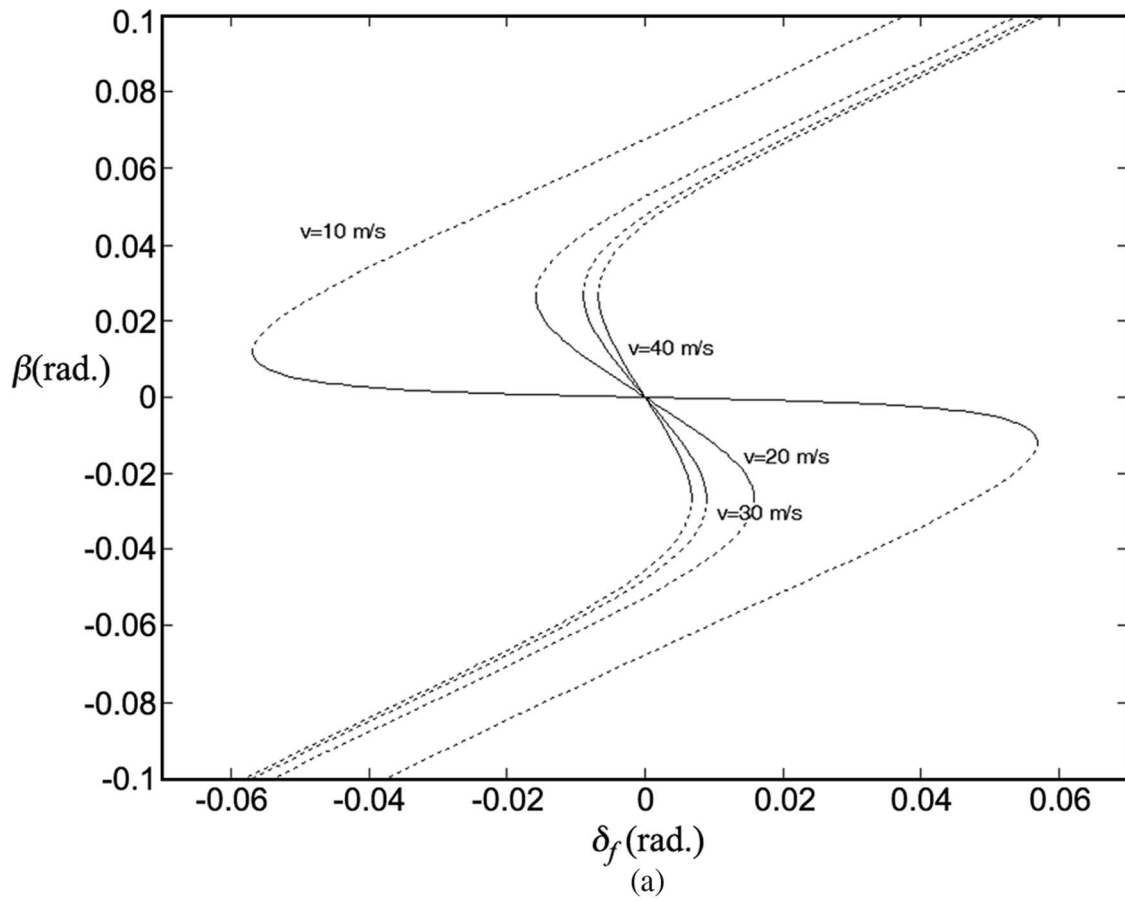


Fig. 3. Bifurcation diagram with respect to different setting of ν . (a) Side-slip angle versus front-wheel angle. (b) Yaw rate versus front-wheel angle.

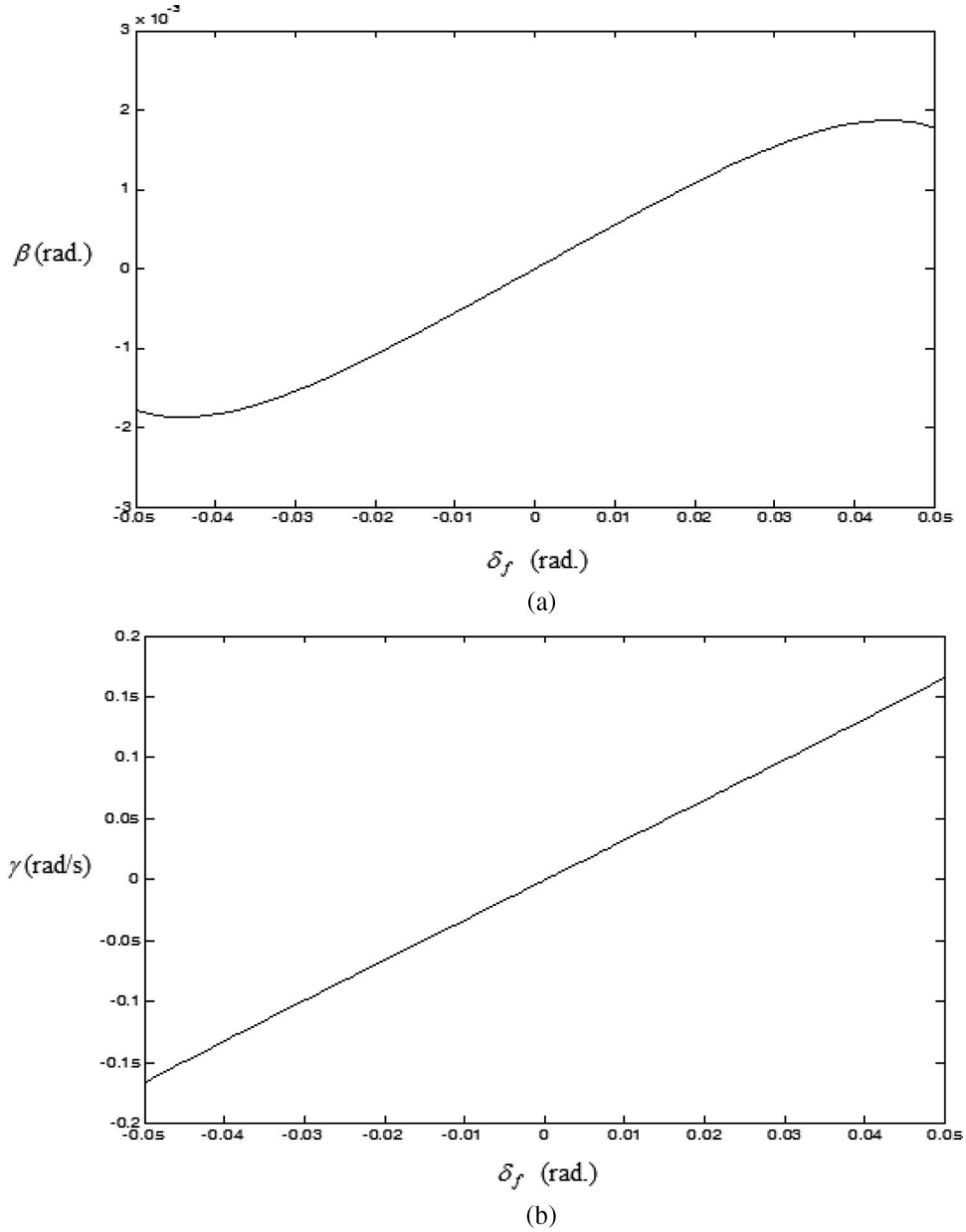


Fig. 4. Equilibrium point valued at $\nu = 9$ m/s. (a) Side-slip angle versus front-wheel angle. (b) Yaw rate versus front-wheel angle.

By applying the Routh–Hurwitz stability criterion, we then have the following stability results.

Lemma 1: The equilibrium point x^0 of system (4), (5) is asymptotically stable if $a_1 + a_4 < 0$ and $a_1a_4 - a_2a_3 > 0$. Here, the a_i s are given in (11)–(14). Moreover, the equilibrium point x^0 is unstable if $a_1 + a_4 > 0$ and $a_1a_4 - a_2a_3 < 0$.

Observation 1: It is known from the so-called “Magic formula” that both values of a_1 and a_4 will generally be negative. An example is given in Section III. Thus, the stability condition in Lemma 1 can then be reduced to where the equilibrium point x^0 of system (4), (5) will be stable if $a_1a_4 - a_2a_3 > 0$ and unstable if $a_1a_4 - a_2a_3 < 0$.

From Observation 1 above, it is clear that the system linearization of (4), (5) at x^0 will in general not have a pair of pure imaginary eigenvalues but might have zero eigenvalue. That means the lateral dynamics of a vehicle system will not

TABLE III
SADDLE-NODE BIFURCATION FOR DIFFERENT SPEEDS

ν (m/s)	Label	δ_f (rad.)	β^0 (rad.)	γ^0 (rad./s)
10	SNBP1	-0.0569	0.0120	-0.2275
	SNBP2	0.0569	-0.0120	0.2275
20	SNBP1	-0.0158	0.0267	-0.1017
	SNBP2	0.0158	-0.0267	0.1017
30	SNBP1	-0.0089	0.0272	-0.0631
	SNBP2	0.0089	-0.0272	0.0631
40	SNBP1	-0.0067	0.0267	-0.0454
	SNBP2	0.0067	-0.0267	0.0454

undergo Hopf bifurcation (e.g., [12]–[14]). However, it might have chance for the appearance of stationary bifurcation at some $\delta_f = \delta_f^0$ such that $a_1a_4 - a_2a_3 = 0$.

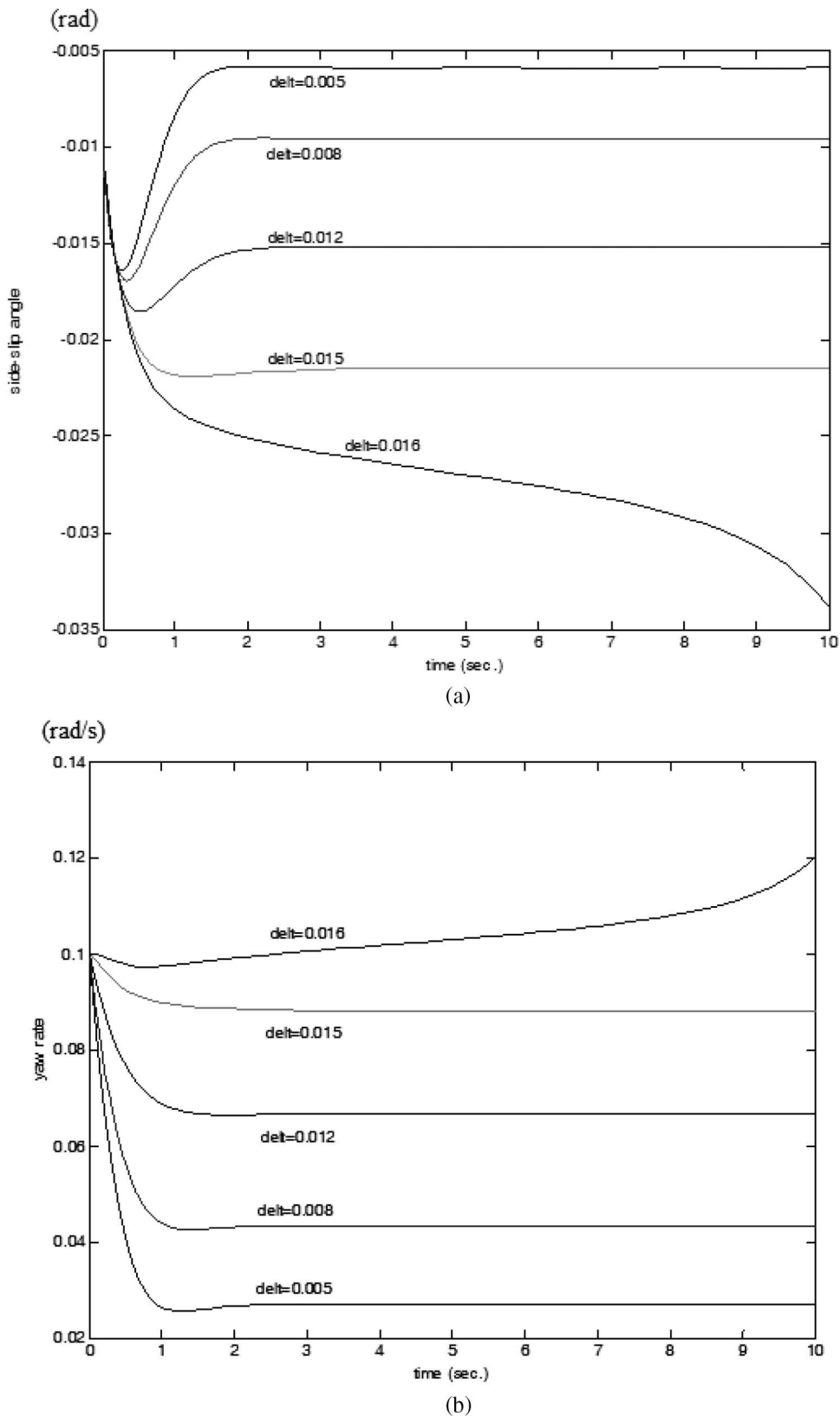
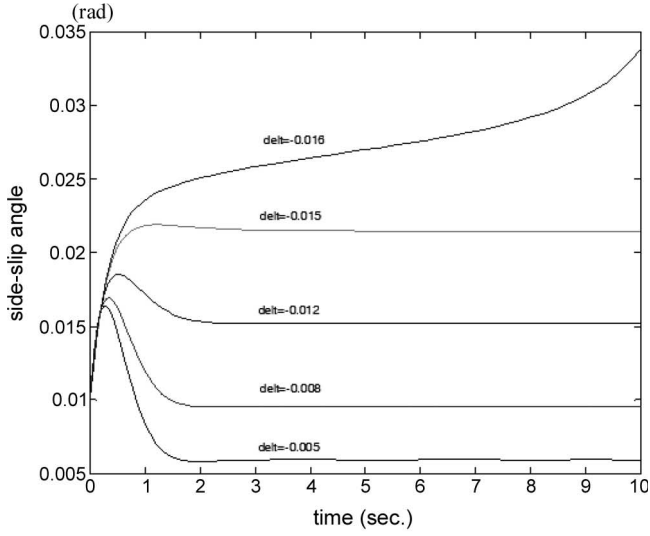


Fig. 5. Time responses with initials: $\beta = -0.01$ rad and $\gamma = 0.1$ rad/s. (a) Side-slip angle β versus time. (b) Yaw rate γ versus time.

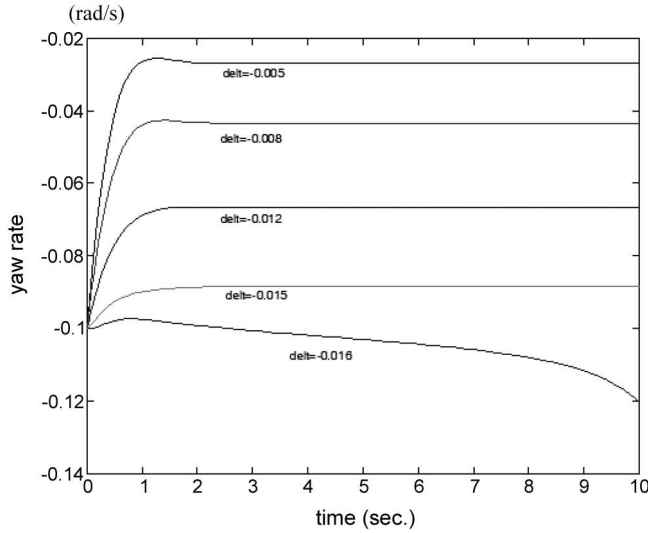
B. Local Bifurcations

In the following, we will discuss the possibility of having a stationary bifurcation (e.g., [11] and [16]) for system (4), (5). Let x^0 be the equilibrium point such that $a_1 a_4 - a_2 a_3 = 0$

with $a_1 < 0$ and $a_4 < 0$. This implies that the linearization of system (4), (5) at x^0 possesses one zero eigenvalue and a stable eigenvalue $\lambda = a_1 + a_4 < 0$. In order to study the possible occurrence of stationary bifurcation for system (4), (5),



(a)



(b)

Fig. 6. Time responses with initials: $\beta = 0.01$ and $\gamma = -0.1$. (a) Side-slip angle β versus time. (b) Yaw rate γ versus time.

we recall the result regarding the existence condition of the so-called “saddle-node bifurcation” from (e.g., [10], [12], and [13]), as presented below.

Consider a class of nonlinear system with the approximation up to the second order in its state x as given by

$$\dot{x} = L_0x + Q_0(x, x) + g\mu. \quad (15)$$

Here, the Jacobian matrix L_0 possesses one zero eigenvalue with remaining eigenvalues lying in the open left-half of the complex plane. The variable μ denotes the system parameter, and $Q_0(x, x)$ denotes the quadratic term in x . Moreover, assume $x = 0$ is an equilibrium point of system (15) at $\mu = 0$.

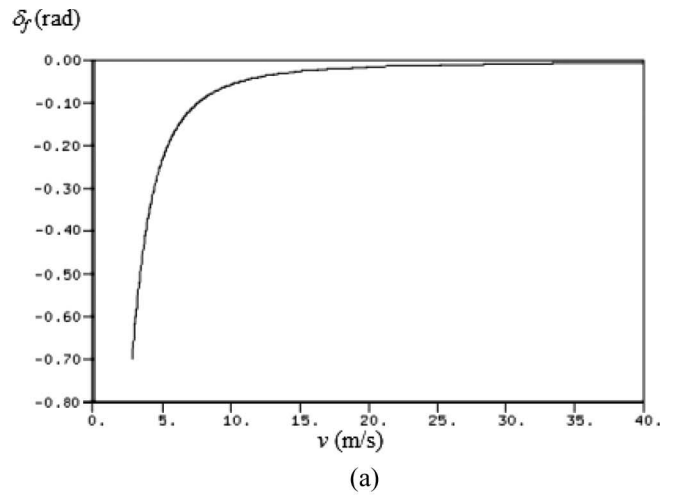
We recall the following lemma (e.g., [10]) regarding the existence conditions of saddle-node bifurcation.

Lemma 2: The equilibrium point $x = 0$ of system (15) will undergo saddle-node bifurcation from the origin at $\mu = 0$ if

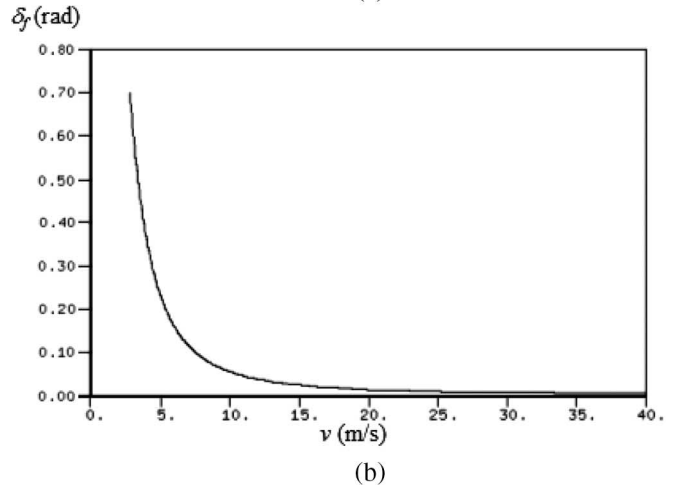
- 1) $lg \neq 0$;
- 2) $lQ_0(r, r) \neq 0$.

TABLE IV
EXISTENCE CONDITION OF THEOREM 1

$a_1 = -2.17032$	$q_{11} = -69.0817$
$a_2 = -1.01782$	$q_{12} = 2.08401$
$a_3 = -3.56284$	$q_{13} = -0.279671$
$a_4 = -1.67372$	$q_{21} = 416.744$
$g_1 = 1.27114$	$q_{22} = -56.0221$
$g_2 = 15.2482$	$q_{23} = 1.90615$
$a_1a_4 - a_2a_3 \approx 0$, with $a_1, a_4 < 0$	
$a_4g_1 - a_2g_2 \approx 13.3924 \neq 0$	
$a_4q_{11} - a_3q_{12} + \frac{a_3^2}{a_4}q_{13} - a_2q_{22} - \frac{a_1^2}{a_2}q_{23} \approx 679.75 \neq 0$	



(a)



(b)

Fig. 7. Saddle-node bifurcation point in $(\delta_f - v)$ space.

Here, l and r denote the left and right eigenvectors corresponding to the zero eigenvalues of L_0 , respectively, with $lr = 1$.

Now, we apply Lemma 2 to the study of local bifurcation for system (4), (5). Define x^0 as the equilibrium point of system (4), (5) with $a_1a_4 = a_2a_3$. Let $\tilde{x} = x - x^0 \triangleq (x_1, x_2)^T$ and $\mu = \delta_f - \delta_f^0$. Taking the Taylor series expansion of the system (4), (5) at (x^0, δ_f^0) , we then have

$$\dot{\tilde{x}} = A\tilde{x} + g\mu + Q(\tilde{x}, \tilde{x}) + O(2) \quad (16)$$

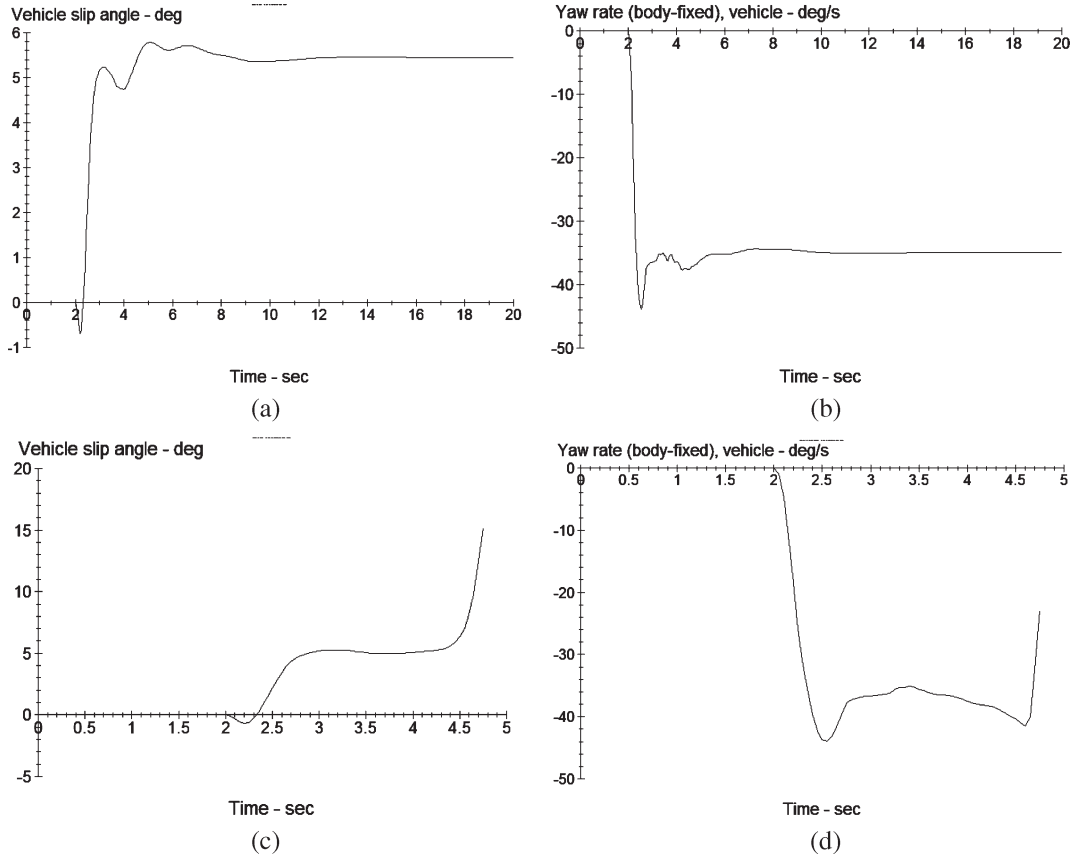


Fig. 8. Vehicle states (a) slip angle and (b) yaw rate before saddle-node point at $\nu = 72$ km/h, $\delta_f = -9.09^\circ$. Vehicle states (c) slip angle and (d) yaw rate after saddle-node point at $\nu = 72$ km/h, $\delta_f = -9.14^\circ$.

where $O(2)$ denotes the remaining second-order term and other high-order terms

$$g \triangleq \begin{bmatrix} g_1 \\ g_2 \end{bmatrix} = \begin{bmatrix} \frac{1}{m\nu} \frac{\partial}{\partial \delta_f} (F_{yf} + F_{yr}) (x^0, \delta_f^0) \\ \frac{\cos \beta^0}{I_z} \frac{\partial}{\partial \delta_f} (L_f F_{yf} - L_r F_{yr}) (x^0, \delta_f^0) \end{bmatrix} \quad (17)$$

and

$$Q(\tilde{x}, \tilde{x}) = \begin{bmatrix} q_{11}x_1^2 + q_{12}x_1x_2 + q_{13}x_2^2 \\ q_{21}x_1^2 + q_{22}x_1x_2 + q_{23}x_2^2 \end{bmatrix}. \quad (18)$$

The Jacobian matrix A is the same as the one in (10) but with $a_1a_4 = a_2a_3$, and the values of q_{ij} are given in Appendix A. From Observation 1, matrix A has one zero eigenvalue and a stable eigenvalue for a general vehicle. In the following, we assume $a_1 < 0$ and $a_4 < 0$ without loss of generality.

Define l and r as the left and right eigenvectors corresponding to the zero eigenvalues of A with $lr = 1$. We then have

$$l = \begin{bmatrix} \frac{a_4}{a_1 + a_4} - \frac{a_2}{a_1 + a_4} \end{bmatrix}$$

and

$$r = \begin{bmatrix} 1 \\ -\frac{a_1}{a_2} \end{bmatrix}^T.$$

It is clear from the relation of $a_1a_4 = a_2a_3$ that we can rewrite r as

$$r = \begin{bmatrix} 1 \\ -\frac{a_3}{a_4} \end{bmatrix}^T.$$

By applying Lemma 2 to system (16), we have

$$l \cdot g = \frac{1}{a_1 + a_4} (a_4g_1 - a_2g_2) \quad (19)$$

and

$$\begin{aligned} lQ_0(r, r) &= \begin{bmatrix} \frac{a_4}{a_1 + a_4} - \frac{a_2}{a_1 + a_4} \\ \left[q_{11} + q_{12} \left(-\frac{a_3}{a_4} \right) + q_{13} \left(-\frac{a_3}{a_4} \right)^2 \right] \\ \left[q_{21} + q_{22} \left(-\frac{a_1}{a_2} \right) + q_{23} \left(-\frac{a_1}{a_2} \right)^2 \right] \end{bmatrix} \\ &= \frac{1}{a_1 + a_4} \left(a_4q_{11} - a_3q_{12} + \frac{a_3^2}{a_4}q_{13} \right. \\ &\quad \left. - a_2q_{21} + a_1q_{22} - \frac{a_1^2}{a_2}q_{23} \right). \quad (20) \end{aligned}$$

The next result follows readily from Lemma 2.

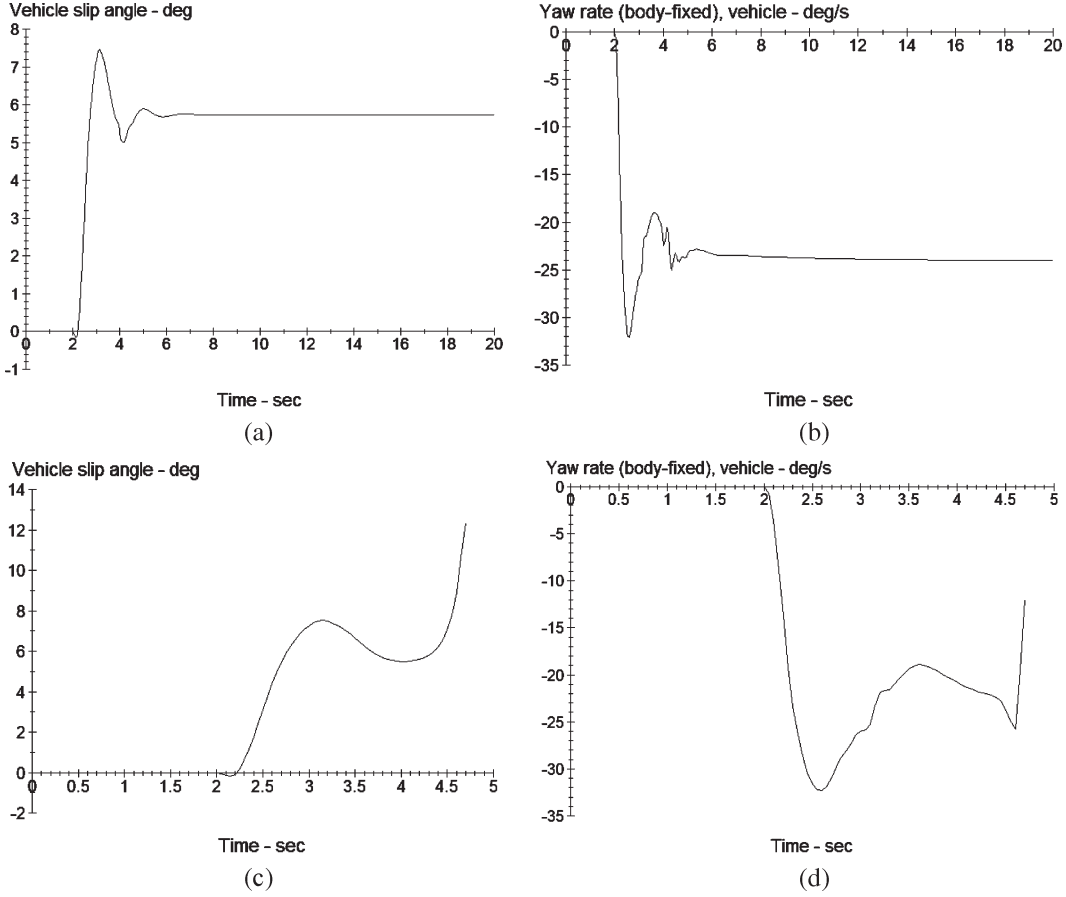


Fig. 9. Vehicle states (a) slip angle and (b) yaw rate before saddle-node point at $\nu = 108$ km/h, $\delta_f = -4.89^\circ$. Vehicle states (c) slip angle and (d) yaw rate after saddle-node point at $\nu = 108$ km/h, $\delta_f = -4.93^\circ$.

Theorem 1: The system (4), (5) will undergo saddle-node bifurcation for the equilibrium point x^0 if the following conditions hold:

- 1) $a_1 a_4 = a_2 a_3$ with $a_1 < 0$ and $a_4 < 0$;
- 2) $a_4 g_1 \neq a_2 g_2$;
- 3) $a_4 q_{11} - a_3 q_{12} + (a_3^2/a_4) q_{13} - a_2 q_{21} + a_1 q_{22} - (a_1^2/a_2) q_{23} \neq 0$.

C. Application to the Vehicle Dynamics With Magic Formula Type Cornering Force

There are many models for cornering force. In this paper, we adopt the well-known ‘‘Magic formula’’ mathematical model (e.g., [7]) for the nonlinear cornering forces F_{yf} and F_{yr} as

$$F_{yf} = D_f \sin \left[C_f \tan^{-1} \left\{ B_f (1 - E_f) \alpha_f + E_f \tan^{-1} (B_f \alpha_f) \right\} \right] \quad (21)$$

$$F_{yr} = D_r \sin \left[C_r \tan^{-1} \left\{ B_r (1 - E_r) \alpha_r + E_r \tan^{-1} (B_r \alpha_r) \right\} \right] \quad (22)$$

where

$$\alpha_f = \beta + \tan^{-1} \left(\frac{L_f}{\nu} r \cdot \cos \beta \right) - \delta_f$$

$$\alpha_r = \beta - \tan^{-1} \left(\frac{L_r}{\nu} r \cdot \cos \beta \right).$$

Here, α_f and α_r denote the slip angle for the front and rear tires, respectively. The approximation relationship between tire slip angles and cornering forces are depicted in Fig. 2.

It is clear from (21) that $x = (\beta, r)^T = (0, 0)^T$ will make $F_{yf} = F_{yr} = 0$ when $\delta_f^0 = 0$. Thus, $x^0 = (0, 0)^T$ is an equilibrium point for system (4), (5) for $\delta_f^0 = 0$. This agrees with the natural behavior of vehicle dynamics. In the following, we first consider to solve the approximation of equilibrium solution about $x^0 = (0, 0)^T$.

It is known that $\theta \approx \tan \theta$, $\sin \theta \approx \theta$, and $\cos \theta \approx 1$ for $\theta \approx 0$. By setting $\dot{x} = 0$ to solve for the equilibrium solution $x^0 = (\beta^0, r^0)^T$ of system (4), (5) near $x^0 = (0, 0)^T$, we have, from (21), that

$$D_f C_f B_f \left(\beta^0 + \frac{L_f}{\nu} r^0 - \delta_f^0 \right) + D_r C_r B_r \left(\beta^0 - \frac{L_r}{\nu} r^0 \right) = m \nu r^0 \quad (23)$$

$$L_f D_f C_f B_f \left(\beta^0 + \frac{L_f}{\nu} r^0 - \delta_f^0 \right) - L_r D_r C_r B_r \left(\beta^0 - \frac{L_r}{\nu} r^0 \right) = 0. \quad (24)$$

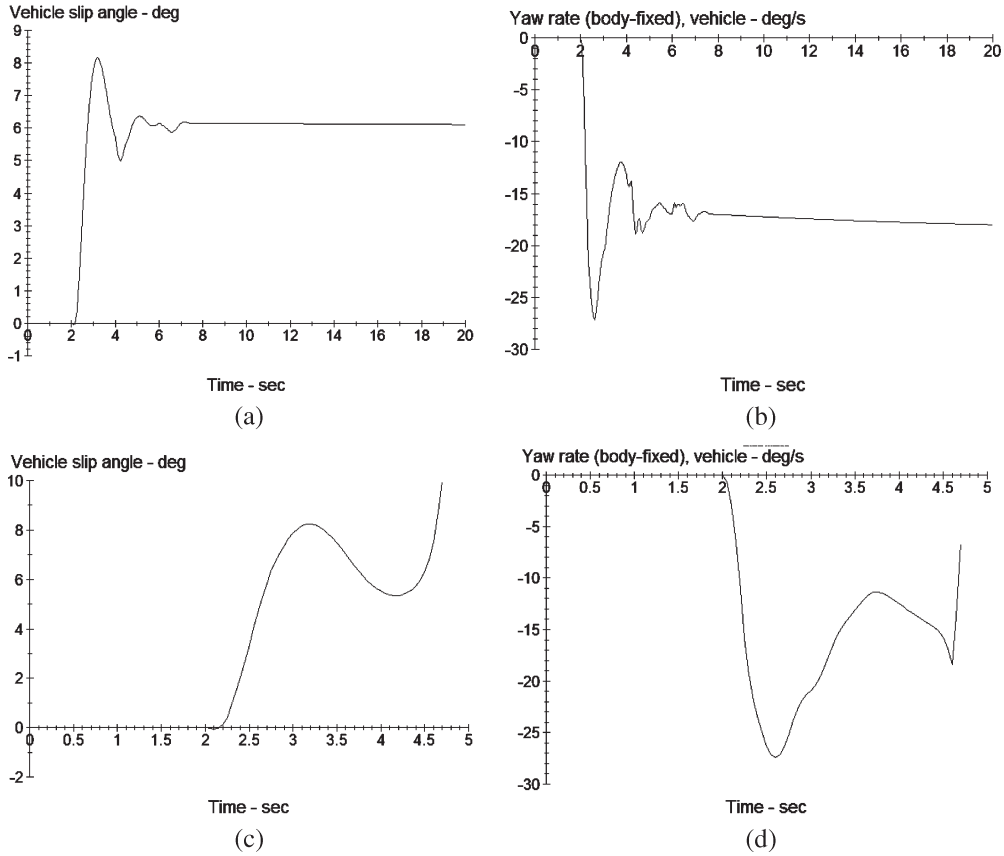


Fig. 10. Vehicle states (a) slip angle and (b) yaw rate before saddle-node point at $\nu = 144$ km/h, $\delta_f = -2.91^\circ$. Vehicle states (c) slip angle and (d) yaw rate after saddle-node point at $\nu = 144$ km/h, $\delta_f = -2.94^\circ$.

By suitable manipulation, we can then rewrite (23) and (24) as

$$(L_f + L_r)D_f C_f B_f \left(\beta^0 + \frac{L_f}{\nu} r^0 - \delta_f^0 \right) = L_r m \nu r^0 \quad (25)$$

and

$$(L_f + L_r)D_r C_r B_r \left(\beta^0 - \frac{L_r}{\nu} r^0 \right) = L_f m \nu r^0. \quad (26)$$

The following observation can be made from (25) and (26).

Observation 2: In general, the values of constants B_f , B_r , C_f , and C_r are positive, while those of D_f and D_r are negative. Example values of these variables will be given in Section IV. Thus, it is not difficult to find from (25) and (26) that the values of β^0 and r^0 will have the same sign if

$$\nu < \nu_{ss} = \sqrt{\frac{-L_r(L_f + L_r)D_r C_r B_r}{L_f m}} \quad (27)$$

and the sign of the sideslip angle β^0 will be opposite from that of the yaw rate r^0 for large axial velocity ν .

Next, we consider the stability of system (4), (5) at the equilibrium point $x^0 = (0, 0)^T$ by using Lemma 1. According to the Magic formula as given in (21) and (22), the values of a_i for the Jacobian matrix A at the equilibrium point

$x^0 = (\beta^0, \gamma^0)^T$ are calculated as those given in Appendix B. For the case of $x^0 = (0, 0)^T$, we have from Observation 2

$$a_1 = \frac{1}{m\nu} (D_f C_f B_f + D_r C_r B_r) < 0 \quad (28)$$

$$a_2 = \frac{1}{m\nu^2} (L_f D_f C_f B_f - L_r D_r C_r B_r) - 1 < 0 \quad (29)$$

$$a_3 = \frac{1}{I_z} (L_f D_f C_f B_f - L_r D_r C_r B_r) > 0 \quad (30)$$

and

$$a_4 = \frac{1}{I_z \nu} (L_f^2 D_f C_f B_f + L_r^2 D_r C_r B_r) < 0. \quad (31)$$

It is clear from (28)–(31) that $a_1 < 0$, $a_2 < 0$, $a_3 > 0$, and $a_4 < 0$ for practical values of B_i , C_i , D_i ($i = f, r$). One example is given in Section IV. These agree with the discussions in Observation 1. The next stability result follows readily from Lemma 1.

Corollary 1: The equilibrium point $x^0 = (0, 0)^T$ for δ_f^0 is asymptotically stable.

Since the equilibrium point $x^0 = (0, 0)^T$ is asymptotically stable, the bifurcation phenomena will not emerge from it. According to (21) and (22), g_i and q_{ij} are also calculated and given in Appendix B. Based on those values of a_i , g_i , and q_{ij} given in Appendix B, it is not difficult to apply Theorem 1 to the study of existence conditions of saddle-node bifurcation for system (4), (5). Numerical examples are given in Section IV for finding such a possibility.

IV. NUMERICAL SIMULATIONS

In this section, we present the numerical study of lateral vehicle dynamics as given in (4) and (5). The selected values of system parameters given in (21) and (22) are the same as those of [6]. Details are given in Tables I and II. In order to verify the study of this paper, the system parameters for low-friction roads are chosen such that the vehicle has a propensity to spin. This could conform the driving condition to that of traveling down hill at constant velocity with equivalent braking effect at zero throttle being applied.

As discussed in Section III, the applied front wheel angle δ_f is treated as a bifurcation parameter. Computer code AUTO [20] is employed to do the numerical analysis since it can numerically calculate the system equilibrium branches by the property of continuity, the eigenvalues of the Jacobian matrix at each equilibrium point, and then determine the corresponding system stability. It is known (e.g., [7], [13], and [14]) that a nonlinear system will have the property of stability exchange before and after the stationary bifurcation point and possess a new system equilibrium branch with respect to the variation of bifurcation parameter. This gives a guide to determine the occurrence of stationary bifurcation and used in AUTO software.

The bifurcation diagram of system (4), (5) with respect to the variation of δ_f is shown in Fig. 3. Note that in Fig. 3, the solid line denotes the stable equilibrium point while the dashed line is for the unstable equilibrium point. As depicted in Fig. 3(a) and (b), the system equilibrium near the origin are all asymptotically stable for different driving speeds ν . This agrees with the analytical result given in Corollary 1. As discussed in Observation 2, the equilibrium values of β and γ will have the same sign if the value of velocity ν is less than $\nu_{ss} \approx 9.5$ m/s. Figs. 3 and 4 demonstrate such results. Saddle-node bifurcation emerging from the equilibrium solution of system (4), (5) is also observed in Fig. 3. The locations of the bifurcation points for different driving speeds, ν are obtained by using AUTO and given in Table III. It is clear from Fig. 3 that the system equilibrium changes stability at the saddle-node bifurcation point and the magnitude of δ_f corresponding to the saddle-node bifurcation becomes smaller as the velocity ν increases.

Note that the equilibrium points within the range of δ_f between the two saddle nodes are stable. It should be pointed out that the equilibrium of sideslip angle is divergent while the yaw rate is convergent for increasing δ_f in the bifurcation diagram. Figs. 5 and 6, respectively, show the time responses for two initial conditions with $\nu = 20$ m/s for different values of δ_f . It can be seen that the vehicle is stable and ends at the value corresponding to the equilibrium point x^0 within the range $|\delta_f| < 0.0158$ rad. It is observed in Figs. 5 and 6 that the system becomes unstable when $|\delta_f| > 0.0158$ rad. This is attributed by the existence of saddle-node bifurcation and its corresponding stability property (e.g., [7], [11], and [12]).

The bifurcation analysis obtained in Section III is employed to verify the numerical results. As given in Table IV, the saddle-node bifurcation point for $\nu = 20$ m/s does satisfy the existence conditions of Theorem 1. Thus, the analytical results presented in Section III will be very helpful in finding possible bifurcation scenarios and system stability. In addition, the location of

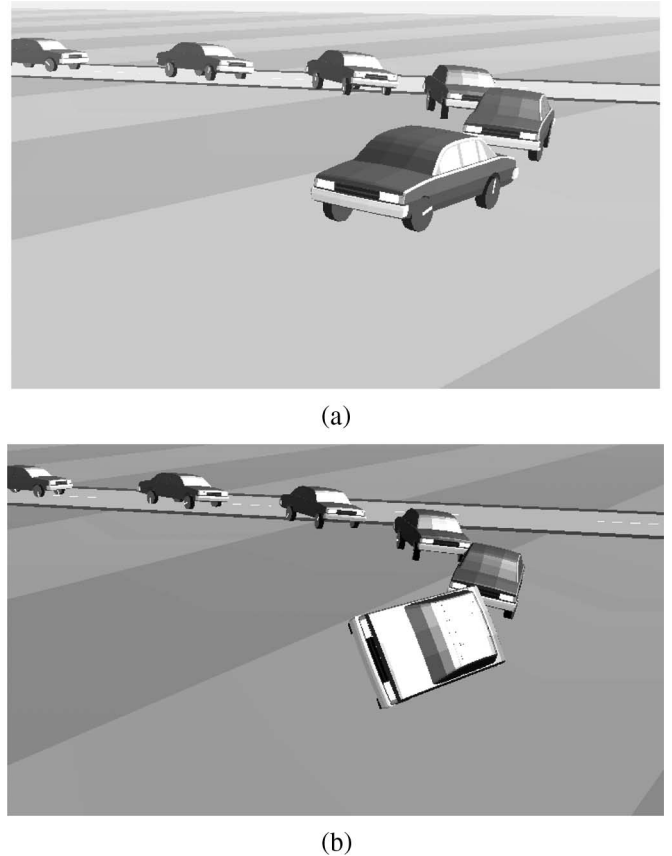


Fig. 11. Vehicle animation at $\nu = 72$ km/h in CarSim (a) before saddle-node bifurcation point ($\delta_f = -9.09^\circ$). (b) After saddle-node bifurcation point ($\delta_f = -9.14^\circ$).

saddle-node bifurcation for values of δ_f with respect to the variation in velocity ν is also given in Fig. 7.

Similar phenomena can be found by using the famous vehicle simulation software CarSim. An example of using the code CarSim to find the occurrence of saddle-node bifurcation is depicted in Figs. 8–10. It is observed from Figs. 8–10 that both slip angle and yaw rate will reach stable values before the saddle-node bifurcation point but become unstable after the bifurcation point for three different values of velocity. Note that all the simulations presented in Figs. 8–10 are obtained by sending the steering command at time $t = 2$ s. Computer animations of the vehicle's behavior before and after the bifurcation point are also obtained using CarSim and depicted in Fig. 11 to demonstrate the existence how the existence of saddle-node bifurcation might affect the vehicle's stability. The location of saddle-node bifurcation in two-parameter space is also obtained as given in Fig. 12.

V. CONCLUSION

In this paper, we focused on the study of stability and non-linear behavior of vehicle lateral dynamics. This is achieved by applying the Routh–Hurwitz stability criterion and bifurcation theory to the second-order model of lateral vehicle dynamics. Without assuming small angles, the stability condition at a given constant velocity for steering systems is also derived, which depends heavily on the cornering force characteristics of

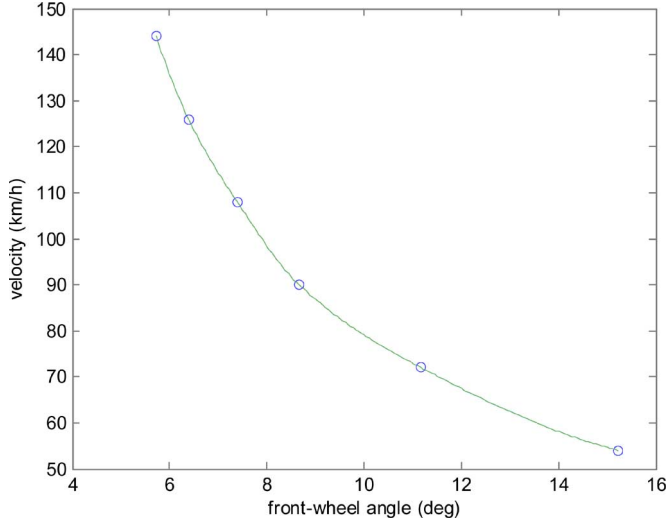


Fig. 12. Saddle-node bifurcation point in $(\nu - |\delta_f|)$ plane for CarSim vehicle model.

the rear tires. Saddle-node bifurcation phenomenon is observed from the equilibrium solution of the nonlinear model, while it never appears in the linear bicycle model (e.g., [3]–[5]). It is found by this paper that the velocity plays a very important role in determining the location of bifurcation points, which is not discussed in the existing results (e.g., [6]). In fact, the value of the applied front wheel angle for the bifurcation points is found to be smaller as the velocity increases. This may provide a partial reason as to why the vehicle steering is hard to control and easily becomes unstable under high speeds.

APPENDIX A

The values of q_{ij} are given as follows:

$$q_{11} = \frac{1}{m\nu} \left(\frac{\partial^2}{\partial \beta^2} (F_{yf} + F_{yr}) (\beta^0, r^0, \delta_f^0) \right)$$

$$q_{12} = \frac{1}{m\nu} \left(\frac{\partial^2}{\partial \beta \partial r} (F_{yf} + F_{yr}) (\beta^0, r^0, \delta_f^0) \right)$$

$$q_{13} = \frac{1}{m\nu} \left(\frac{\partial^2}{\partial r^2} (F_{yf} + F_{yr}) (\beta^0, r^0, \delta_f^0) \right)$$

$$q_{21} = \frac{1}{I_z} \left(\left(\frac{\partial^2}{\partial \beta^2} L_f F_{yf} (\beta^0, r^0, \delta_f^0) - \frac{\partial^2}{\partial \beta^2} L_r F_{yr} (\beta^0, r^0, \delta_f^0) \right) \cos \beta^0 - 2 \cdot \left(\frac{\partial}{\partial \beta} L_f F_{yf} (\beta^0, r^0, \delta_f^0) - \frac{\partial}{\partial \beta} L_r F_{yr} (\beta^0, r^0, \delta_f^0) \right) \sin \beta^0 \right)$$

$$q_{22} = \frac{1}{I_z} \left(\left(\frac{\partial^2}{\partial \beta \partial r} L_f F_{yf} (\beta^0, r^0, \delta_f^0) - \frac{\partial^2}{\partial \beta \partial r} L_r F_{yr} (\beta^0, r^0, \delta_f^0) \right) \cos \beta^0 - \left(\frac{\partial}{\partial r} L_f F_{yf} (\beta^0, r^0, \delta_f^0) - \frac{\partial}{\partial r} L_r F_{yr} (\beta^0, r^0, \delta_f^0) \right) \sin \beta^0 \right)$$

$$q_{23} = \frac{1}{I_z} \left(\frac{\partial^2}{\partial r^2} L_f F_{yf} (\beta^0, r^0, \delta_f^0) - \frac{\partial^2}{\partial r^2} L_r F_{yr} (\beta^0, r^0, \delta_f^0) \right) \cos \beta^0.$$

APPENDIX B

The values of a_i and g_i are shown at the bottom of the page and are continued on the next page, where ν , m , I_z , L_j , B_j , C_j , D_j , E_j ($j = f, r$) are as defined in previous sections.

$$a_1 = \frac{1}{m\nu} \left(D_f \cos [C_f \tan^{-1} \{ B_f(1 - E_f)\alpha_f(\beta^0, r^0, \delta_f^0) + E_f \tan^{-1} (B_f\alpha_f(\beta^0, r^0, \delta_f^0)) \}] \cdot \left[\frac{C_f}{1 + (B_f(1 - E_f)\alpha_f(\beta^0, r^0, \delta_f^0) + E_f \tan^{-1} (B_f\alpha_f(\beta^0, r^0, \delta_f^0)))^2} \right] \cdot \left[B_f(1 - E_f) + \frac{E_f B_f}{1 + (B_f\alpha_f(\beta^0, r^0, \delta_f^0))^2} \right] \cdot \left[1 - \frac{\frac{L_f}{\nu} r^0 \sin \beta^0}{1 + (\frac{L_f}{\nu} r^0 \cos \beta^0)^2} \right] + D_r \cos [C_r \tan^{-1} \{ B_r(1 - E_r)\alpha_r(\beta^0, r^0) + E_r \tan^{-1} (B_r\alpha_r(\beta^0, r^0)) \}] \cdot \left[\frac{C_r}{1 + (B_r(1 - E_r)\alpha_r(\beta^0, r^0) + E_r \tan^{-1} (B_r\alpha_r(\beta^0, r^0)))^2} \right] \cdot \left[B_r(1 - E_r) + \frac{E_r B_r}{1 + (B_r\alpha_r(\beta^0, r^0))^2} \right] \cdot \left[1 + \frac{\frac{L_r}{\nu} r^0 \sin \beta^0}{1 + (\frac{L_r}{\nu} r^0 \cos \beta^0)^2} \right] \right)$$

$$\begin{aligned}
a_2 &= \frac{1}{m\nu} \left(D_f \cos [C_f \tan^{-1} \{B_f(1 - E_f)\alpha_f(\beta^0, r^0, \delta_f^0) + E_f \tan^{-1}(B_f\alpha_f(\beta^0, r^0, \delta_f^0))\}] \right. \\
&\quad \cdot \left[\frac{C_f}{1 + (B_f(1 - E_f)\alpha_f(\beta^0, r^0, \delta_f^0) + E_f \tan^{-1}(B_f\alpha_f(\beta^0, r^0, \delta_f^0)))^2} \right] \\
&\quad \cdot \left[B_f(1 - E_f) + \frac{E_f B_f}{1 + (B_f\alpha_f(\beta^0, r^0, \delta_f^0))^2} \right] \cdot \left[\frac{\frac{L_f}{\nu} \cos \beta^0}{1 + (\frac{L_f}{\nu} r^0 \cos \beta^0)^2} \right] \\
&\quad + D_r \cos [C_r \tan^{-1} \{B_r(1 - E_r)\alpha_r(\beta^0, r^0) + E_r \tan^{-1}(B_r\alpha_r(\beta^0, r^0))\}] \\
&\quad \cdot \left[\frac{C_r}{1 + (B_r(1 - E_r)\alpha_r(\beta^0, r^0) + E_r \tan^{-1}(B_r\alpha_r(\beta^0, r^0)))^2} \right] \\
&\quad \cdot \left[B_r(1 - E_r) + \frac{E_r B_r}{1 + (B_r\alpha_r(\beta^0, r^0))^2} \right] \cdot \left[-\frac{\frac{L_r}{\nu} \cos \beta^0}{1 + (\frac{L_r}{\nu} r^0 \cos \beta^0)^2} \right] \Big) - 1 \\
a_3 &= \frac{\cos \beta}{I_z} \left(L_f D_f \cos [C_f \tan^{-1} \{B_f(1 - E_f)\alpha_f(\beta^0, r^0, \delta_f^0) + E_f \tan^{-1}(B_f\alpha_f(\beta^0, r^0, \delta_f^0))\}] \right. \\
&\quad \cdot \left[\frac{C_f}{1 + (B_f(1 - E_f)\alpha_f(\beta^0, r^0, \delta_f^0) + E_f \tan^{-1}(B_f\alpha_f(\beta^0, r^0, \delta_f^0)))^2} \right] \\
&\quad \cdot \left[B_f(1 - E_f) + \frac{E_f B_f}{1 + (B_f\alpha_f(\beta^0, r^0, \delta_f^0))^2} \right] \cdot \left[1 - \frac{\frac{L_f}{\nu} r^0 \sin \beta^0}{1 + (\frac{L_f}{\nu} r^0 \cos \beta^0)^2} \right] \\
&\quad - L_r D_r \cos [C_r \tan^{-1} \{B_r(1 - E_r)\alpha_r(\beta^0, r^0) + E_r \tan^{-1}(B_r\alpha_r(\beta^0, r^0))\}] \\
&\quad \cdot \left[\frac{C_r}{1 + (B_r(1 - E_r)\alpha_r(\beta^0, r^0) + E_r \tan^{-1}(B_r\alpha_r(\beta^0, r^0)))^2} \right] \\
&\quad \cdot \left[B_r(1 - E_r) + \frac{E_r B_r}{1 + (B_r\alpha_r(\beta^0, r^0))^2} \right] \cdot \left[1 + \frac{\frac{L_r}{\nu} r^0 \sin \beta^0}{1 + (\frac{L_r}{\nu} r^0 \cos \beta^0)^2} \right] \Big) \\
a_4 &= \frac{\cos \beta}{I_z} \left(L_f D_f \cos [C_f \tan^{-1} \{B_f(1 - E_f)\alpha_f(\beta^0, r^0, \delta_f^0) + E_f \tan^{-1}(B_f\alpha_f(\beta^0, r^0, \delta_f^0))\}] \right. \\
&\quad \cdot \left[\frac{C_f}{1 + (B_f(1 - E_f)\alpha_f(\beta^0, r^0, \delta_f^0) + E_f \tan^{-1}(B_f\alpha_f(\beta^0, r^0, \delta_f^0)))^2} \right] \\
&\quad \cdot \left[B_f(1 - E_f) + \frac{E_f B_f}{1 + (B_f\alpha_f(\beta^0, r^0, \delta_f^0))^2} \right] \cdot \left[\frac{\frac{L_f}{\nu} \cos \beta^0}{1 + (\frac{L_f}{\nu} r^0 \cos \beta^0)^2} \right] \\
&\quad - L_r D_r \cos [C_r \tan^{-1} \{B_r(1 - E_r)\alpha_r(\beta^0, r^0) + E_r \tan^{-1}(B_r\alpha_r(\beta^0, r^0))\}] \\
&\quad \cdot \left[\frac{C_r}{1 + (B_r(1 - E_r)\alpha_r(\beta^0, r^0) + E_r \tan^{-1}(B_r\alpha_r(\beta^0, r^0)))^2} \right] \\
&\quad \cdot \left[B_r(1 - E_r) + \frac{E_r B_r}{1 + (B_r\alpha_r(\beta^0, r^0))^2} \right] \cdot \left[-\frac{\frac{L_r}{\nu} \cos \beta^0}{1 + (\frac{L_r}{\nu} r^0 \cos \beta^0)^2} \right] \Big) \\
g_1 &= \frac{1}{m\nu} \left(D_f \cos [C_f \tan^{-1} \{B_f(1 - E_f)\alpha_f(\beta^0, r^0, \delta_f^0)\}] \right. \\
&\quad \cdot \left[\frac{C_f}{1 + (B_f(1 - E_f)\alpha_f(\beta^0, r^0, \delta_f^0) + E_f \tan^{-1}(B_f\alpha_f(\beta^0, r^0, \delta_f^0)))^2} \right] \\
&\quad \cdot \left[-B_f(1 - E_f) - \frac{E_f B_f}{1 + (B_f\alpha_f(\beta^0, r^0, \delta_f^0))^2} \right] \Big) \\
g_2 &= \frac{L_f \cos \beta}{I_z} \left(D_f \cos [C_f \tan^{-1} \{B_f(1 - E_f)\alpha_f(\beta^0, r^0, \delta_f^0)\}] \right. \\
&\quad \cdot \left[\frac{C_f}{1 + (B_f(1 - E_f)\alpha_f(\beta^0, r^0, \delta_f^0) + E_f \tan^{-1}(B_f\alpha_f(\beta^0, r^0, \delta_f^0)))^2} \right] \\
&\quad \cdot \left[-B_f(1 - E_f) - \frac{E_f B_f}{1 + (B_f\alpha_f(\beta^0, r^0, \delta_f^0))^2} \right] \Big)
\end{aligned}$$

ACKNOWLEDGMENT

The authors would like to thank the reviewers and the Associate Editor for their helpful and detailed comments, which have helped to improve the presentation of this paper.

REFERENCES

- [1] A. Vahidi and A. Eskandarian, "Research advances in intelligent collision avoidance and adaptive cruise control," *IEEE Trans. Intell. Transp. Syst.*, vol. 4, no. 3, pp. 143–153, Sep. 2003.
- [2] L. Li, F. Y. Wang, and Q. Zhou, "Integrated longitudinal and lateral tire/road friction modeling and monitoring for vehicle motion control," *IEEE Trans. Intell. Transp. Syst.*, vol. 7, no. 1, pp. 1–19, Mar. 2006.
- [3] J. Ackerman, J. Guldner, W. Sienel, R. Steinhauser, and V. I. Utkin, "Linear and nonlinear controller design for robust automatic steering," *IEEE Trans. Control Syst. Technol.*, vol. 3, no. 1, pp. 132–143, Mar. 1995.
- [4] H. Peng and M. Tomizuka, "Vehicle lateral control for highway automation," in *Proc. Amer. Control Conf.*, San Diego, CA, May 23–25, 1990, pp. 788–794.
- [5] H. Peng, T. Hessburg, M. Tomizuka, and W. Zhang, "A theoretical and experimental study on vehicle lateral control," in *Proc. Amer. Control Conf.*, Chicago, IL, Jun. 24–26, 1992, pp. 1738–1742.
- [6] E. Ono, S. Hosoe, H. D. Tuan, and S. Doi, "Bifurcation in vehicle dynamics and robust front wheel steering control," *IEEE Trans. Control Syst. Technol.*, vol. 6, no. 3, pp. 412–420, May 1998.
- [7] L. R. Ray, "Nonlinear state and tire force estimation for advanced vehicle control," *IEEE Trans. Control Syst. Technol.*, vol. 3, no. 1, pp. 117–124, Mar. 1995.
- [8] J. E. Naranjo, C. Gonzalez, R. Garcia, T. Pedro, and R. E. Haber, "Power-steering control architecture for automatic driving," *IEEE Trans. Intell. Transp. Syst.*, vol. 6, no. 4, pp. 406–415, Dec. 2005.
- [9] L. Beji and Y. Bestaoui, "Motion generation and adaptive control method of automated guided vehicles in road following," *IEEE Trans. Intell. Transp. Syst.*, vol. 6, no. 1, pp. 113–123, Mar. 2005.
- [10] N. Kopell and L. N. Howard, "Bifurcations and trajectories joining critical points," *Adv. Math.*, vol. 18, pp. 306–358, 1975.
- [11] E. H. Abed and J. H. Fu, "Local feedback stabilization and bifurcation control, II. Stationary bifurcation," *Syst. Control Lett.*, vol. 8, no. 5, pp. 467–473, May 1987.
- [12] J. Guckenheimer and P. Holmes, *Nonlinear Oscillations, Dynamical Systems, and Bifurcations of Vector Fields*. New York: Springer-Verlag, 1983.
- [13] S. N. Chow and J. K. Hale, *Methods of Bifurcation Theory*. New York: Springer-Verlag, 1992.
- [14] L. N. Howard, "Nonlinear oscillation," in *Nonlinear Oscillations in Biology*, F. C. Hoppendeadt, Ed. Providence, RI: Amer. Math. Soc., 1979, pp. 1–67.
- [15] D.-C. Liaw and E. H. Abed, "Stabilization of tethered satellites during station-keeping," *IEEE Trans. Autom. Control*, vol. 35, no. 11, pp. 1186–1196, Nov. 1990.
- [16] D.-C. Liaw and E. H. Abed, "Active control of compressor stall inception: A bifurcation-theoretic approach," *Automatica*, vol. 32, no. 1, pp. 109–115, 1996.
- [17] D.-C. Liaw and C.-C. Song, "Analysis of longitudinal flight dynamics: A bifurcation-theoretic approach," *J. Guid. Control Dyn.*, vol. 24, no. 1, pp. 109–116, 2001.
- [18] D.-C. Liaw, K.-H. Fang, and C.-C. Song, "Bifurcation analysis of power systems with tap changer," in *Proc. IEEE ICNSC*, Tucson, AZ, Mar. 19–22, 2005, pp. 283–288.
- [19] J. Y. Wong, *Theory of Ground Vehicles*. Hoboken, NJ: Wiley, 2001.
- [20] E. J. Doedel, "AUTO: A program for the automatic bifurcation analysis of autonomous systems," *Congressus Numerantium*, vol. 30, pp. 265–284, 1981.
- [21] *CarSim User Manual*, Mech. Simul. Corp., Ann Arbor, MI, 2001, Version 5.11.



Der-Cherng Liaw (S'86–M'90–SM'02) received the B.S. degree in control engineering from National Chiao Tung University (NCTU), Hsinchu, Taiwan, R.O.C., in 1982, the M.S. degree in electrical engineering from National Taiwan University, Taipei, Taiwan, in 1985, and the Ph.D. degree in electrical engineering from the University of Maryland, College Park, in 1990.

During 1990–1991, he was a Postdoctoral Fellow with the Institute of Systems Research, University of Maryland. Since August 1991, he has been with the NCTU, Hsinchu, where he is currently a Professor of electrical and control engineering. His research interests include nonlinear control systems, spacecraft control, singular perturbation methods, bifurcation control, jet engine control, flight control, electric power systems and power electronics, radio frequency identification (RFID), and implementation issues.

Dr. Liaw served as a Designated Assistant to the Associate Editor for the IEEE TRANSACTIONS ON AUTOMATIC CONTROL during 1990–1992. He was also a member of Editorial Board of 1993 American Control Conference.



Hsin-Han Chiang (S'02–M'03) received the B.S. degree in electrical and control engineering from National Chiao Tung University (NCTU), Hsinchu, Taiwan, R.O.C., in 2001, where he is currently working toward the Ph.D. degree in electrical and control engineering.

His research interests include intelligent systems and control theory, fuzzy systems and control, automated vehicle control, and intelligent transportation systems.



Tsu-Tian Lee (M'87–SM'89–F'97) was born in Taipei, Taiwan, R.O.C., in 1949. He received the B.S. degree in control engineering from the National Chiao Tung University (NCTU), Hsinchu, Taiwan, R.O.C., in 1970 and the M.S. and Ph.D. degrees in electrical engineering from the University of Oklahoma, Norman, in 1972 and 1975, respectively.

In 1975, he was appointed as an Associate Professor and, in 1978, as a Professor and Chairman of the Department of Control Engineering, NCTU. In 1981, he became a Professor and Director of the

Institute of Control Engineering, NCTU. In 1986, he was a Visiting Professor and, in 1987, a Full Professor of electrical engineering with the University of Kentucky, Lexington. In 1990, he was a Professor and Chairman of the Department of Electrical Engineering, National Taiwan University of Science and Technology (NTUST), Taipei, Taiwan, R.O.C. In 1998, he became a Professor and Dean of the Office of Research and Development, NTUST. In 2000, he was appointed as a Chair Professor with the Department of Electrical and Control Engineering, NCTU. Since 2004, he has been with the National Taipei University of Technology, Taipei, where he is currently the President.

Prof. Lee was elected as a Fellow of the Institution of Electrical Engineers in 2000. He became a Fellow of the New York Academy of Sciences in 2002. He has served as a member of the Technical Program Committee and a member of the Advisory Committee for many IEEE sponsored international conferences. He is now the Vice President for Conferences of the IEEE Systems, Man, and Cybernetics Society. He received the Distinguished Research Award from the National Science Council, Taiwan, R.O.C., in 1991–1998; the Academic Achievement Award in Engineering and Applied Science from the Ministry of Education, Taiwan, R.O.C., in 1997; the National Endow Chair from the Ministry of Education, Taiwan, R.O.C., in 2003 and 2006, respectively; and the TECO Science and Technology Award from TECO Technology Foundation in 2003.